Salicylic Acid Affects Root Meristem Patterning via Auxin Distribution in a Concentration-Dependent Manner[1]

Taras Pasternak,[a,2] Edwin P. Groot,[d,2] Fedor V. Kazantsev,[b,c] William Teale,[a] Nadya Omelyanchuk,[b,c] Vasilina Kovrizhnykh,[b,c] Klaus Palme,[a,e,f,3,4] and Victoria V. Mironova[b,c,3,4]

[a]Institute for Biology II, Albert-Ludwigs-University Freiburg, D-79104 Freiburg, Germany
[b]Institute of Cytology and Genetics, Novosibirsk 630090, Russia
[c]Novosibirsk State University, Novosibirsk 630090, Russia
[d]State Key Laboratory of Crop Biology, Shandong Agricultural University, Tai'An 271018, China
[e]BIOSS Centre for Biological Signalling Studies, Albert-Ludwigs-University Freiburg, D-79104 Freiburg, Germany
[f]Center for Biosystems Analysis, Albert-Ludwigs-University Freiburg, D-79104 Freiburg, Germany

ORCID IDs: 0000-0001-5061-4076 (T.P.); 0000-0002-2728-3835 (K.P.); 0000-0003-3438-0147 (V.V.M.).

The phytohormone salicylic acid (SA) is well known for its induction of pathogenesis-related proteins and systemic acquired resistance; SA also has specific effects on plant growth and development. Here we analyzed the effect of SA on Arabidopsis (*Arabidopsis thaliana*) root development. We show that exogenous SA treatment at low (below 50 μM) and high (greater than 50 μM) concentrations affect root meristem development in two different PR1-independent ways. Low-concentration SA promoted adventitious roots and altered architecture of the root apical meristem, whereas high-concentration SA inhibited all growth processes in the root. All exposures to exogenous SA led to changes in auxin synthesis and transport. A wide range of SA treatment concentrations activated auxin synthesis, but the effect of SA on auxin transport was dose dependent. Mathematical modeling of auxin synthesis and transport predicted auxin accumulation or depletion in the root tip following low- or high-concentration SA treatments, respectively. SA-induced auxin accumulation led to the formation of more layers of columella initials, an additional cortical cell layer (middle cortex), and extra files of epidermis, cortex, and endodermis cells. Suppression of SHORT ROOT and activation of CYCLIN D6;1 mediated the changes in radial architecture of the root. We propose that low-concentration SA plays an important role in shaping root meristem structure and root system architecture.

In plants, mobile peptides, nucleic acids, proteins, and endogenous metabolites mediate a complicated network of growth responses to developmental and environmental cues. The action of salicylic acid (SA; 2-hydroxybenzoic acid) is a part of these diverse responses (for review, see Rivas-San Vicente and Plasencia, 2011). However, research into the signaling pathways initiated by SA has mainly focused on its role in plant defense and immunity (for review, see Vlot et al., 2009). High exogenous concentrations (here defined as > 50 μM) of SA stimulate systemic acquired resistance (SAR), a vitally important adaptive immunity response that protects against a broad spectrum of pathogens (Mur et al., 2006; Fu and Dong, 2013).

SA is a natural phenolic compound that is present in Arabidopsis (*Arabidopsis thaliana*) tissues between 0.25 and 1 $\mu g.g^{-1}$ of fresh weight (Rivas-San Vicente and Plasencia, 2011). When challenged with a pathogen, SA accumulates rapidly in distal leaves to concentrations of 3 $\mu g.g^{-1}$, with local SA concentrations at wounded regions reaching 20 $\mu g.g^{-1}$ (Zhang et al., 2010). *PATHOGENESIS-RELATED GENE 1* (*PR1*) gene expression is commonly used as a marker for SA-mediated SAR activation; *PR1* transcription is rapidly induced in leaves upon both pathogen exposure and exogenous SA treatment (Uknes et al., 1992).

Accordingly, the majority of investigations into the molecular mechanisms of SA action on Arabidopsis have been performed using exogenous concentrations of between 150 μM and 1 mM (e.g. Iglesias et al., 2011; Fu et al., 2012; Van der Does et al., 2013; Armengot et al., 2014). At these concentrations, SA signaling is regulated by NONEXPRESSOR OF PATHOGENESIS RELATED GENES 1 (NPR1), a major regulator of SAR (Cao et al., 1997; Fu and Dong, 2013). SA binds directly to NPR3 and NPR4, which controls NPR1 stability (Fu et al., 2012). A number of other participants in SA-signaling pathways have been described; however their exact roles remain unclear (for review, see Vlot et al., 2009; Fu and Dong, 2013).

In addition to biotic stresses, SA mediates the responses to abiotic stresses, such as drought, low temperature, and high salinity (Miura and Tada, 2014). Although relatively poorly understood, an important role for SA in plant development is supported by published data. There is evidence that SA regulates seed production and germination, vegetative growth, flower formation, and senescence (for review, see Rivas-San Vicente and Plasencia, 2011).

The role of SA as a developmental regulator has mainly been studied in nonmodel plants. Generally, low concentrations of applied SA promote plant

growth under unfavorable conditions, whereas high SA concentrations inhibit growth; the threshold between low and high concentrations depends on plant species and the method of treatment. SA exhibited growth-promoting (50 μM) and growth-inhibiting (250 μM) properties on chamomile (*Matricaria chamomilla*) seedlings (Kovácik et al., 2009). Presowing of wheat (*Triticum aestivum*) grains in 10 μM SA solution increased fresh and dry plant weight, whereas presowing in 1 mM SA reduced these parameters (Hayat et al., 2005). Mustard plants (*Brassica juncea*) sprayed with 10 μM SA solution had higher seed yield and dry mass, but 100 μM SA and higher did not provide these effects (Fariduddin et al., 2003). Between 25 and 75 μM SA improves somatic embryogenesis in carrot (*Daucus carota*), whereas higher SA concentrations are detrimental for it (Hosseini et al., 2011).

Comparatively less is known about the role of SA in development of plant roots. Exogenous SA proportionally reduces Arabidopsis root elongation (Pasternak et al., 2005; Zhao et al., 2015) and specifically induces its waving in a dose-dependent manner (Zhao et al., 2015). Within a concentration range of up to 50 μM exogenous SA, the maximal amplitude of root waving is reached at 30 μM. Exogenous treatment with 250 μM SA inhibits Arabidopsis primary root growth and lateral root development (Armengot et al., 2014). However, in a number of plant species, lower SA concentrations induced an increase in root biomass: in corn (*Zea mays*) after 1.5 μM SA treatment (Agtuca et al., 2013); in soybean (*Glycine max*) seedlings sprayed with 10 nM, 100 μM, or 10 mM SA (Gutiérrez-Coronado et al., 1998); in *Pinus patula* sprayed with 10 nM and 1 μM SA (San-Miguel et al., 2003). Even femtomolar SA concentrations were found inductive for lateral root growth in *Catharanthus roseus* (Echevarría-Machado et al., 2007). Between 200 and 400 μM SA promoted adventitious root formation in mung bean (*Vigna radiate*) hypocotyl cuttings, but an increased concentration (800 μM) inhibited this process (Yang et al., 2013). An inhibitory effect of SA-deficiency on root meristem activity and root elongation was reported in rice (*Oryza sativa*; Xu et al., 2017). The molecular nature of SA effects on root development is largely unknown, but it may be mediated by changes in auxin signaling and auxin transport (Pasternak et al., 2005; Du et al., 2013; Armengot et al., 2014; Zhao et al., 2015).

Here we investigate the role and nature of SA response in root growth and development. First, we studied the effect of different concentrations of exogenous SA on Arabidopsis root morphology and anatomy and showed that low and high dosages affect the root meristem structure in principally different ways. By applying experimental and computational approaches we reveal that the diverse phenotypic effects are mediated by either auxin accumulation or auxin depletion in the meristem. We show that SA-mediated auxin accumulation leads to increase in the number of periclinal and tangential divisions in the root outer layers via a *CYCD6;1*-dependent mechanism. We propose two bioactive concentration windows for SA: at low levels it acts as a developmental regulator and at high levels it acts as a stress hormone.

RESULTS

Exogenous SA Inhibits Primary and Lateral Root Growth, But Activates Formation of Adventitious Roots in a Concentration-Dependent Manner

In order to analyze how externally applied SA affected Arabidopsis root development at different doses, 3 d after germination (dag) seedlings were transferred to media containing SA concentrations of between 3 and 200 μM for 5 d. At all concentrations tested, SA significantly reduces the length of the primary root (Fig. 1, A and B) due to inhibition of cell elongation (Fig. 1C). Exogenous SA below 50 μM leads to gradual inhibition of the root growth, but treatments above 50 μM arrest root growth soon after transfer (Fig. 1A). Upon transfer of these 8 dag plants back to control medium, some of the roots regained growth, e.g. after 150 μM SA half of the roots recovered and continued growing.

Externally applied SA inhibited lateral root development (Fig. 1, B and D). Despite similar number of lateral root primordia initiated after SA exposure, some of them stopped developing from stage IV on (Supplemental Fig. S1). No lateral root primordia emerged from the root portion grown after transfer to SA at $\geq$20 μM and less lateral root primordia emerged from the root portion grown before the transfer.

Plants treated by relatively low concentrations of SA (3–50 μM) developed adventitious roots more

[1]This work was supported by Bundesministerium für Forschung und Technologie (German Ministry for Research and Technology) (BMBF SYSTEC; BMBF FKZ031B0503B and 031B0556); Deutsche Forschungsgemeinschaft (DFG), the Excellence Initiative of the German Federal and State Governments (EXC 294); Deutsche Forschungsgemeinschaft (DFG) German Research Foundation (SFB746, INST 39/839,840,841); and Deutsches Zentrum für Luft- und Raumfahrt (German Centre for Air and Space Travel) (DLR 50WB1022). Russian participants were supported by the Russian Science Foundation. Image analysis, statistical analysis, and overall management of the project were supported by RSF 18-74-10008. Mathematical modelling was supported by RSF 17-74-10102. Support was also provided by the Shandong "Foreign experts double hundred" Program (WST2017008, to E.G.)

[2]These authors contributed equally to this article.

[3]Senior author.

[4]Author for contact: victoria.v.mironova@gmail.com

The author responsible for distribution of materials integral to the findings presented in this article in accordance with the policy described in the Instructions for Authors (www.plantphysiol.org) is: Victoria V. Mironova (victoria.v.mironova@gmail.com).

T.P., E.P.G., K.P., and V.V.M. conceived and designed the study; T.P. acquired experimental data; F.V.K. and V.V.M. performed computational analysis and mathematical modeling; W.T., N.O., V.K., K.P., and V.V.M. analyzed the data; T.P., N.O., and V.V.M. drafted the article; E.P.G., W.T., and K.P. revised the article.

www.plantphysiol.org/cgi/doi/10.1104/pp.19.00130

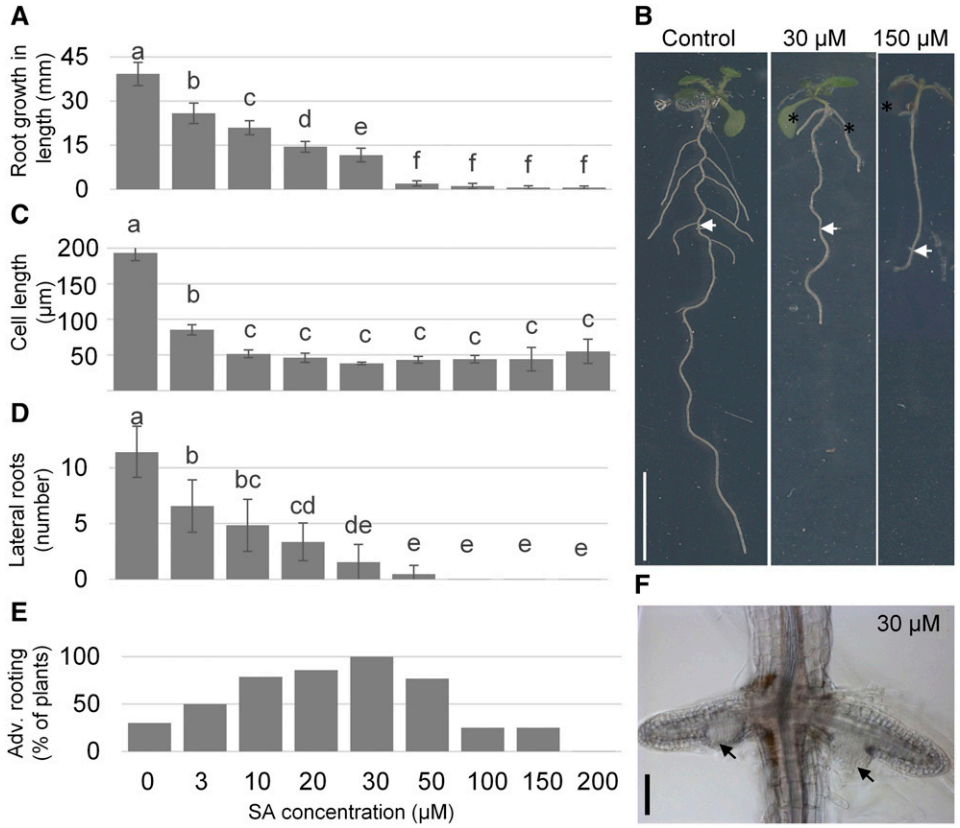

Figure 1. Concentration-dependent effect of exogenous SA on Arabidopsis (*Arabidopsis thaliana*) root growth. A–E, Analysis of the changes in root growth induced by different SA concentrations after transfer to SA-containing plates at 3 dag for 5 d. A, Primary root growth in length, after transfer to the new medium. B, Morphology of the seedlings treated by 30 and 150 μM SA for 5 d, analyzed in A and C–E. White arrows indicate where the root end was located after transfer. C, The length of epidermal cell in the mature zone. D, The number of lateral roots. E, The portion of plants with at least one adventitious (Adv.) root. F, The root-to-shoot junction of the seedling treated by 30 μM SA for 5 d. The secondary adventitious root primordia are shown by black arrows. A, C, and D, Error bars depict SD; statistical groups indicated by letters were determined by one-way ANOVA with Tukey post hoc test (CI 95%, n = 15–25). Scale bars = 1 cm (B) and 100 μm (F).

frequently than control plants (Fig. 1E); sometimes even secondary adventitious roots were observed (Fig. 1F). After 5 d of SA treatment at 30 μM, all plants had developed adventitious roots.

The ANOVA of morphological changes (Fig. 1A, C, and D; Supplemental Fig. S1) identified that SA concentrations below and above 50 μM have different effects on the growth of primary, lateral, and adventitious roots in Arabidopsis. We next studied the effects of relatively low (30 μM) and high (150 μM) SA concentrations in more detail.

Exogenous SA Alters Root Meristem Structure

We analyzed the cellular architecture in the root tip of seedlings grown on either low or high SA media (Fig. 2). A progressive inhibition of the proximal meristem was observed with increasing SA concentration: at 30 μM the meristem slightly reduced in size (Fig. 2B), and at 150 μM the top meristem border was barely detectable, because all cells were much bigger than control ones (Fig. 2C). In accordance, we observed a gradual decrease in *CYCB1;1 (CYCLIN B1;1)* expression (Fig. 3A). More than half of the roots transferred to 150 μM SA did not show any *CYCB1;1* signal.

The exogenous SA effect on the distal meristem was concentration dependent (Fig. 2). The low concentration SA treatment led to enlargement of the distal meristem. After 5-d treatment with 30 μM SA, the distal meristem acquired between two and four extra tiers of small cells with compact nuclei and lacking starch granules (Fig. 2, B and D). The distal meristem was also enlarged in width, with barely identifiable cortex/endodermis and epidermis/Lateral Root Cap (LRC) initials, whose division planes and division frequency apparently were disturbed. In contrast, the organization of the distal meristem grown at 150 μM seemed unaffected, aside from bigger cells and lack of starch granules in the columella (Fig. 2, C and D).

The extra tiers of the distal meristem formed under 30 μM SA expressed both quiescent center (QC; WOX5:GFP, WUSCHEL-RELATED HOMEOBOX 5 promoter driving GFP) and columella initial cell (J2341) markers (Fig. 3, C and D). However, WOX5:GFP expression in the extra tiers was less intense compared with that in the QC (Fig. 3C).

SA Effects on the Root Meristem Are Spatially Distinct from PR1 Induction

High concentrations of SA activate PR1-dependent SA response (Fu and Dong, 2013), which takes part in pathogen resistance. We next asked whether the observed SA effects on the root meristem are also mediated through a PR1-dependent pathway. Using *PR1::GUS* plants, we found that application of either low or high levels of SA led to activation of *PR1* expression; however, this expression was localized almost exclusively to the mature zone of the root (Fig. 3B). PR1-dependent transcription was absent in the root meristem of both control and

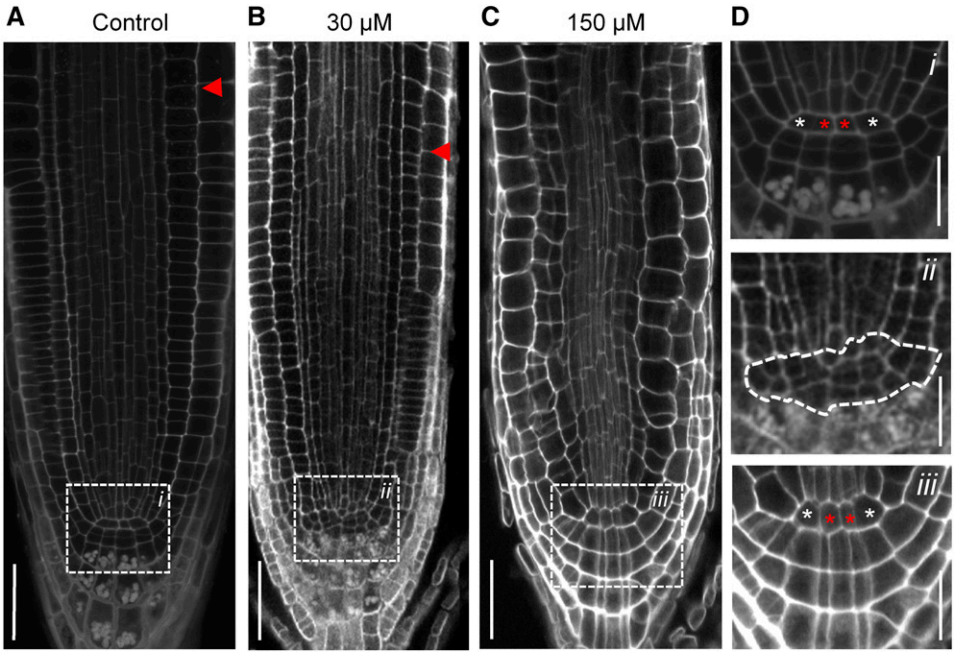

Figure 2. Exogenous SA significantly alters root meristem architecture. A–C, Root tip anatomy after 72 h of growth on mock (A), 30 μM SA (B), or 150 μM SA (C) medium. Red arrowheads indicate the end of the proximal meristem. In D, enlargements of the dashed rectangles from A–C are shown. D*ii*, white outline with QC, columella, cortex/endodermis, epidermis/LRC initial cells. D*i* and *iii*, red asterisks mark the QC, and white mark cortex/endodermis initials. Scale bars = 50 μm.

SA-treated plants, even at the high dosage of 150 μM SA. Thus, only the mature zone of the root is capable of initiating PR1 expression, and SA alters root meristem structure by a yet unknown PR1-independent mechanism.

SA Alters Auxin Distribution in the Root Apical Meristem

Induction of adventitious roots and enlargement of the distal meristem have in common the key role of auxin. Auxin accumulates already in early derivatives of the adventitious root founder cell (Della Rovere et al., 2013). Local auxin levels control maintenance or differentiation of cells in the distal root meristem (Ding and Friml, 2010). We therefore analyzed the distribution of auxin-dependent signaling in plants in the presence of SA.

Exogenous SA affected *DR5*-dependent GFP fluorescence depending on concentration: low-level SA activated *DR5* activity and high-level SA inhibited it

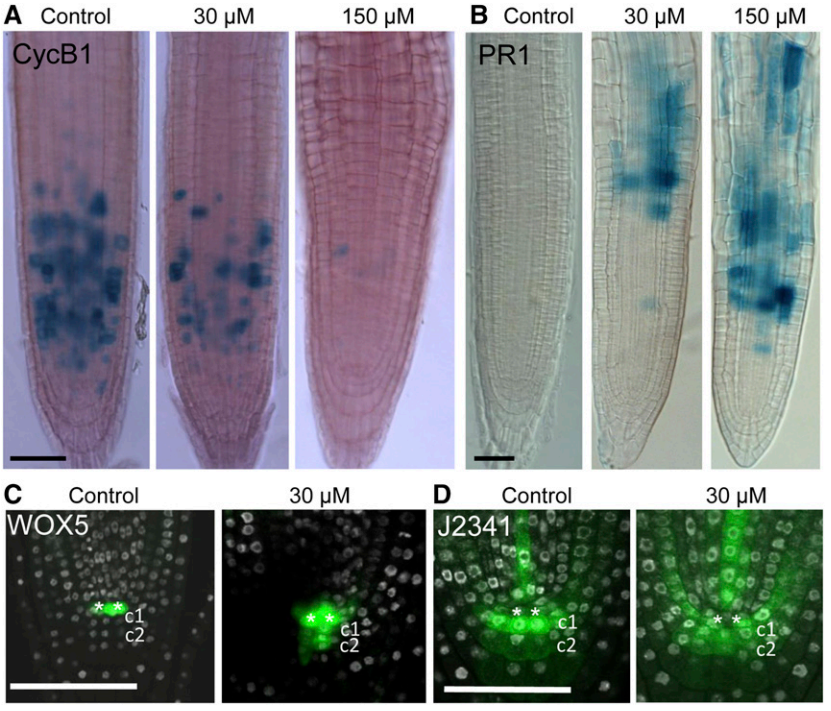

Figure 3. Exogenous SA affects expression of meristem markers in a PR1-independent manner. A and B, The root tips of plants grown on the media containing 0, 30, and 150 μM SA for 36 h. A, *CYCB1::GUS*. B: *PR1::GUS* plants. C and D, Control roots and roots exposed to 30 μM SA for 72 h. The green GFP signal is counterstained with DAPI in white. White asterisks mark the QC position, c1 the first columella tier (columella initials), and c2 the second columella tier. The green signal is *WOX5:GFP* in (C), and the J2341 enhancer trap line in (D). Scale bars = 50 μm.

(Fig. 4, A and B). Measurements of the fluorescent signals in the root tips showed a 2-fold increase of *DR5*-dependent fluorescent protein intensity after 36 h of 30 μM SA exposure and a quarter decrease after 150 μM SA (Fig. 4E). A time course shows that the increase in *DR5*-dependent GFP fluorescence was observed after 6 h of 30 μM SA treatment, before any phenotypic changes became visible (Fig. 4A). *DR5* activity was also significantly enhanced in the mature root zone of 30 μM SA-exposed plants (Supplemental Fig. S2, A and B). Instead of local auxin response maxima at presumptive lateral root primordia, the auxin response increased along the mature zone of 30 μM SA-treated roots. These results led us to hypothesize that exogenous SA might affect auxin transport and/or metabolism in the root.

To test this hypothesis, we analyzed expression of the auxin efflux proteins PIN1 (PIN-FORMED 1), PIN2, PIN4, PIN7, and the auxin biosynthetic enzyme TAA1 (TRP AMINOTRANSFERASE OF ARABIDOPSIS 1) after 36 h of SA treatment using antibodies and reporter lines. The semiquantitative and qualitative analyses indicated that SA affects both auxin synthesis and auxin transport. TAA1 expression increased 3-fold in the root tips exposed to either low or high SA concentrations (Fig. 4, D and E). In addition, SA exposure leads to an increase in TAA1 expression level with a reduction of the TAA1 expression domain in the distal elongation zone (Supplemental Fig. S2E). Different levels of SA had similar effects on the expression of PIN2 and PIN7; they were inhibited almost 2-fold (Fig. 4, C and E); PIN4 expression was not changed (data not shown). Intriguingly, the expression of PIN1 was differentially regulated: 30 μM SA up-regulated PIN1 by 30%, but 150 μM SA inhibited it by 40% (Fig. 4, C and E).

Computer Simulation of Auxin Distribution in the Root Apical Meristem under SA Treatment

The experimental results (Fig. 4E) indicate that SA has four inputs in the auxin distribution system: SA activates de novo auxin synthesis and rootward auxin

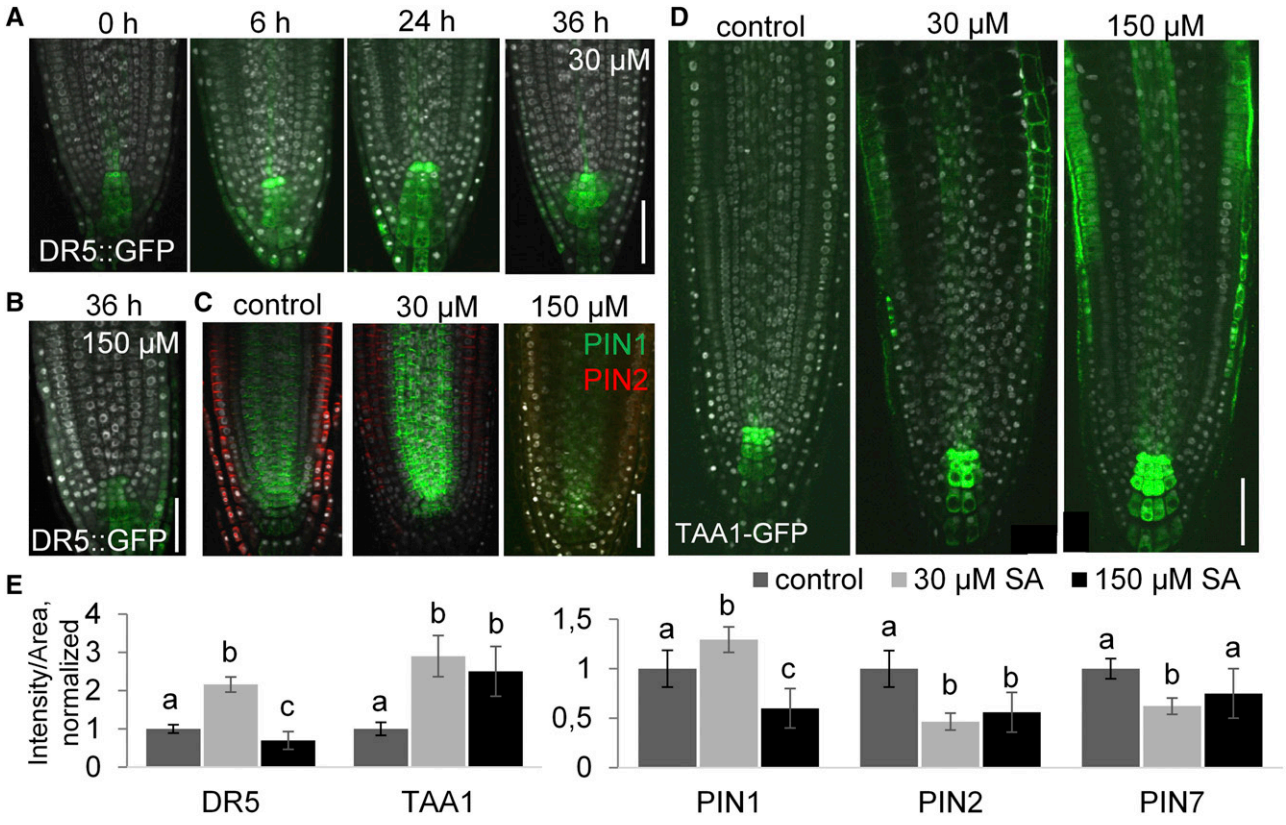

Figure 4. SA treatment changes auxin distribution in the root tip. A, *DR5::GFP* signal gradually increases in the root tip over a 24-h time course of exposure to 30 μM SA. After 24 h the fluorescence intensity persisted, but the expression domain enlarged. B, 150 μM SA downregulates *DR5::GFP* in the root tip. C, Immunolabeling of PIN1 and PIN2: both low and high SA dosages downregulate PIN2, whereas PIN1 is activated by low SA and downregulated by high SA. D, SA upregulates expression of *TAA1::TAA1-GFP*. A–D, counterstained with DAPI. E, Quantitative reporter intensity measurement in root tips after 24 h exposure to 30 μM (light gray) or 150 μM SA (black). The relative fluorescence intensities per area are presented for SA-treated and control (dark gray) root tips. The measurements were obtained from *DR5::GFP*, *TAA1::TAA1-GFP*, *PIN1::PIN1-GFP*, *PIN2::PIN2-GFP*, and *PIN7::PIN7-GFP* plants. Error bars depict SD. Statistical groups indicated by letters were determined by one-way ANOVA with Tukey post hoc test (CI 95%, n = 10–15). Scale bars = 50 μm.

transport, but down-regulates nonpolar and shootward auxin transport in the root tip. The exogenous SA effect on rootward transport is concentration dependent. We used mathematical modeling to predict the changes in auxin distribution in the root tip resulting from SA-mediated inputs.

In order to do this, we adapted an established mathematical model of auxin action in the root meristem (Mironova et al., 2012; Hong et al., 2017). The model (Fig. 5A) allows reconstructing longitudinal patterning of auxin and PINs in the root meristem in silico, just from considering the feedback regulations between auxin and PINs (Fig. 5B) without the necessity to prespecify PIN expression domains. Depending on the rates of auxin synthesis and transport, the model generates, moves, or dissipates the distal auxin maximum, crucial for maintenance of the QC and the distal meristem, together with adjustment of PIN expression domains.

We introduced SA-dependent multipliers into the initial model to replicate the effects of exogenous SA on auxin transport ($k^{SA_{PIN}}$) and auxin biosynthesis ($k^{SA_{TAA1}}$; Fig. 5, B and C; Supplemental Text). The SA effect was then analyzed in a two-step computer simulation. We first started the model simulation from uniform auxin distribution ($[a]_j$=1) without considering the SA effect ($k^{SA_{PIN}} = k^{SA_{TAA1}}$=1). The resulting "control" steady-state auxin pattern had its concentration maximum in the central cell layers, four rows proximal to the root tip (Fig. 5D; Supplemental Fig. S3).

To simulate SA treatment, we used the control steady state as a starting point, and changed $k^{SA_{PIN}}$ and $k^{SA_{TAA1}}$ according to the experimental data (Fig. 4E). In case of low-level SA, we set the synthesis rates of PIN1, PIN2, PIN7, and TAA1 multipliers of 1.3, 0.5, 0.6, and 3, respectively (Fig. 5B; Supplemental Text). Simulation gave a new steady-state solution, with the same auxin maximum position. However, the strength of the auxin maximum was significantly increased when compared with that from the control solution (Fig. 5E; Supplemental Fig. S3). Maintenance of the distal auxin maximum position was restricted to a narrow parameter space of the model (Supplemental Figs. S4–S6; Mironova et al., 2012); thus, the present solution under significant changes in the parameter settings is an unexpected finding.

Simulation of high-level SA exposure (Fig. 5C) gave the steady-state solution with weaker and displaced auxin maximum (Supplemental Fig. S4). The model outcome matches the experimental data when we decreased the intensity of auxin inflow into the meristem by 45%–60% in addition to $k^{SA_{PIN}}$ and $k^{SA_{TAA1}}$ (Fig. 5F).

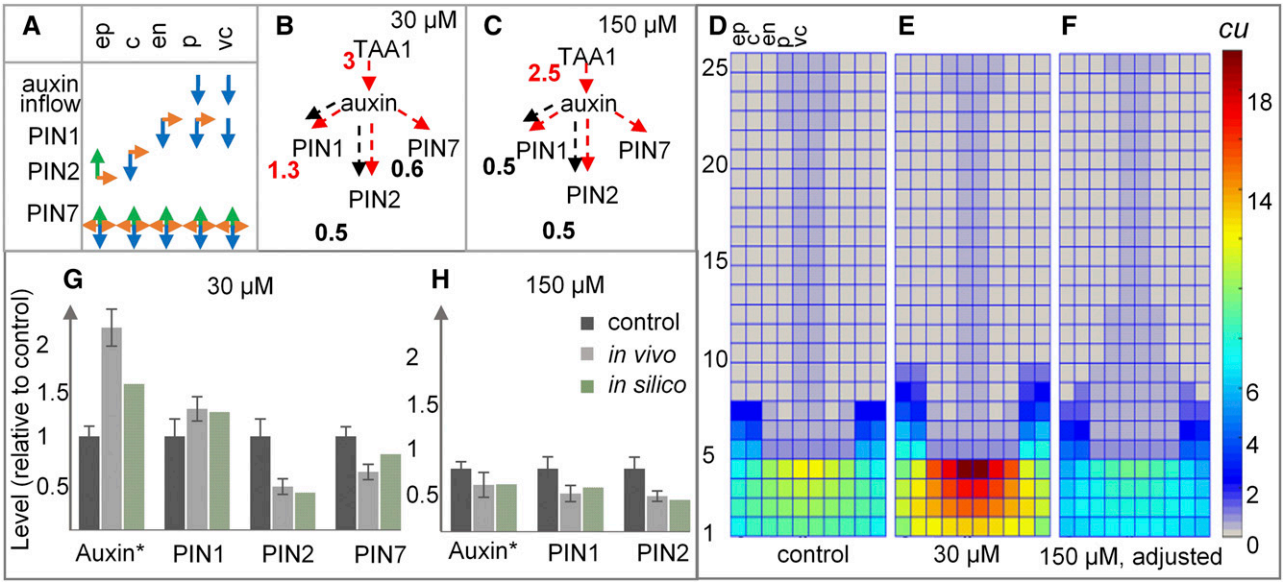

Figure 5. Mathematical modeling of auxin distribution in the root meristem after SA exposure. A, The direction of auxin flow mediated by different PINs in the mathematical model (ep, epidermis; c, cortex; en, endodermis; p, pericycle; vc, vascular cells). Blue arrows, acropetal; green, basipetal; orange, lateral. Auxin inflow from the differentiated tissues to the meristem is assigned to the proximal meristem boundary only. B and C, Variables and their regulations considered in the mathematical model. Dashed arrows depict the feedbacks from the initial model (Mironova et al., 2012). The multipliers show the simulated effect of 30 μM SA (B) or 150 μM SA (C) on the variables according to the experimental data (Fig. 4E). PIN7 at 150 μM SA was too variable to be significant, and the multiplier was set to 1. Red arrows, positive regulation; black arrows, negative regulation. D–F, Stationary solutions along a longitudinal section of control (D) and SA-treated root tips (E and F). *cu*, Concentration units. E, generated using multipliers from B. F, generated using multipliers from C and with 50% decreased auxin inflow. G and H, Comparison of stationary solutions (green) with the experimental data (light gray) on GFP fluorescence of *DR5::GFP* (titled "Auxin*"), *PIN1::PIN1-GFP*, *PIN2::PIN2-GFP*, and *PIN7::PIN7-GFP* root tips after 36 h treatment by 30 μM SA (G) and 150 μM SA (H). Both in silico and in vivo data were normalized to their respective controls (dark gray column). Error bars for dark and light gray columns depict SD.

The shoots of the seedlings grown on the 150 μM SA were indeed smaller compared with that of control plants, suggesting that they synthesize less auxin, decreasing auxin flow from the shoot.

To test the model's outcomes we compared the SA treatment in silico and in vivo: namely, control ratios for auxin and PINs levels calculated in the model with the ratios measured for the corresponding reporter lines (Fig. 4E) after 36 h of either low or high levels of SA treatment. The analysis gave quantitative agreement of the model calculations with the experimental data (Fig. 5, G and H; Supplemental Text). We therefore conclude that the model adequately reproduced the changes in auxin distribution after exposure to SA.

SA Induces Middle Cortex Formation and Tangential Divisions in Cortex and Epidermis

After verification of the model, we examined the model predictions. When low-level SA treatment was simulated, the stronger auxin maximum, which might be responsible for enlargement of the distal meristem, was not the only change in auxin distribution. Auxin amounts in the outer cell layers (epidermis, endodermis, and cortex) of the SA-treated in silico root were higher, whereas the auxin amounts in vascular cells were lower in comparison with that resulting from the control solution (Fig. 6A). We hypothesized that these changes in auxin patterning may alter the root meristem morphology activating cell proliferation in the outer layers and inhibiting it in the stele.

We therefore undertook a closer examination of the root meristem structure exposed to low-level SA using iRoCS Toolbox for three-dimensional analysis (Schmidt et al., 2014; Fig. 6, C, D, F, and G; Supplemental Fig. S7, A–D). In accordance with the predictions (Fig. 6A), we revealed multiple cases of extra cell divisions in the outer layers. In epidermis and cortex, extra divisions were radially oriented, resulting in the formation of new cell files (Fig. 6, C and D; Supplemental Fig. S7, A and C). In addition, treatment with 30 μM SA disturbed

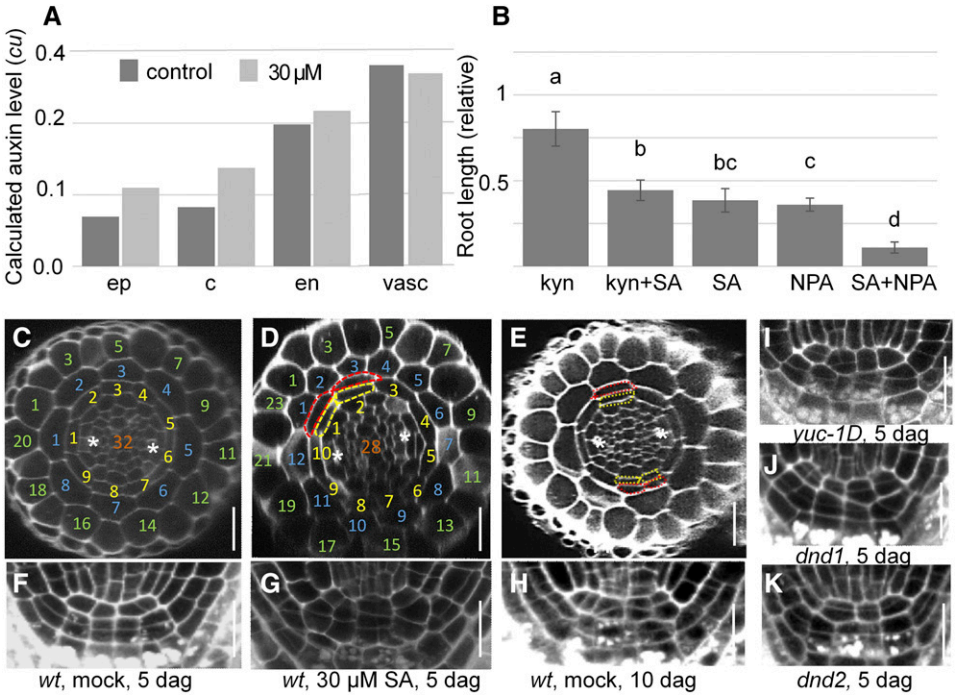

Figure 6. SA affects longitudinal and radial structure via modulation of auxin distribution. A, Model predicts auxin accumulation in the outer layers (epidermis [ep], cortex [c], endodermis [en]) and depletion in the vascular tissues (vasc) for treated by 30 μM SA root tips. Histogram shows predicted auxin amount in concentration units (*cu*). B, Primary root elongation relative to control, after transfer to the new medium at 3 dag for 5 d: one-half strength Murashige and Skoog supplemented with mock, 5 μM *l*-kynurenine (kyn), 5 μM NPA, and 30 μM SA in various combinations. Error bars depict SD; statistical groups indicated by letters were determined by one-way ANOVA with Tukey post hoc test (CI 95%, n = 15–20). C–H, Anatomical structure of the root tips in the wild-type (wt) 5 dag (C and F), 5 dag upon 30 μM SA exposure (D and G), and 10 dag (E and H) seedlings. Transverse (C–E) and longitudinal (F–H) sections of roots. C, Control root contains 32 vascular, 9 endodermis (yellow), 8 cortex (blue), and 8 trichoblast (green) cell files. The white asterisks indicate protophloem cells. D, Increase in the number of cell files in endodermis, cortex, and epidermis under 30 μM SA; decrease in the number of vascular cell files. Periclinal cell divisions in endodermis yield middle cortex (red) and endodermis (yellow) cells. E, Middle cortex naturally forms in older seedlings of 10 dag. G–K, Disturbance in divisions of cortex/endodermis initials and the QC in the roots of 5 dag wild-type seedlings upon 30 μM SA exposure (G), 10 dag wild-type seedlings (H), *yuc-1D* transgenic 5 dag seedlings (I), and SA-accumulating 5 dag mutants *dnd1* and *dnd2* (J and K). Scale bars = 25 μm.

patterning of the endodermis-cortex initials and led to precocious formation of the middle cortex, a second cortical cell layer (Fig. 6D; Supplemental Fig. S7, A–C). Ectopic periclinal divisions in endodermal cells were detected as early as after 36 h of 30 μM SA treatment in 5 dag seedlings, and their number increased over time. The radial number of endodermal cells also increased (Fig. 6D; Supplemental Fig. S7D). Accordingly, 8 dag 30 μM SA-treated plants had an intercalary middle-cortex layer; 10 endodermis and 12 cortex cell files ($n = 10$) instead of the 8 to 9 seen in the control ($n = 15$); and up to 30 epidermal cell files after SA treatment instead of the 20–24 seen in control roots (Fig. 6, C and D). Consistent with predicted auxin level (Fig. 6A), the number of cell files in the vascular cylinder was lower in roots exposed to SA: 24–28 instead of 30–34 cell files in the control (Fig. 6, C and D).

By Inducing Auxin Accumulation, Low-Level SA Promotes Root Meristem Maturation

Study of the model with respect to parameters shows that three inputs, TAA1 activation, PIN1 activation, and PIN7 inhibition, are equally important for providing a stable and strengthened distal auxin maximum under low-level SA (Supplemental Figs. S5 and S6). Down-regulation of PIN2 has less effect. We analyzed root growth in seedlings transferred to the solid medium containing auxin synthesis inhibitor (5 μM *l*-kynurenine) or auxin transport inhibitor (5 μM napthylphthalamic acid [NPA]) with or without 30 μM SA (Fig. 6B). The inhibitory action of NPA on root growth was similar to low-level SA, but together these substances gave a synergistic effect. In contrast, *l*-kynurenine treatment partially recovered root growth under low-level SA, despite *l*-kynurenine being a growth inhibitor. This data support the idea that SA modulates auxin distribution to affect root meristem activity.

Analysis of the model with respect to the parameters also identified that the model is most sensitive to the intensity of auxin flow into the vascular cells at the meristematic boundary (Supplemental Fig. S5). The position of the auxin maximum maintains in a narrow interval of the intensity changes, moving upward upon flow increase and downward upon decrease (Supplemental Fig. S5E). In addition, auxin concentration in the endodermis is proportional to auxin inflow changes. We hypothesized that we might find an enlarged distal meristem and middle-cortex formation in the root meristem upon certain conditions.

An increase in the rate of auxin flow into the root meristem may occur in vivo in older seedlings (Bhalerao et al., 2002). The root meristem is a dynamic structure, changing during maturation of the plant (Baum et al., 2002). Indeed, three-dimensional analysis of the root tips of 10 dag control plants identified dividing QC and disturbed division planes in cortex/endodermis initials in 40% of tested plants ($n = 20$; Fig. 6H). In 60% of these plants, we also observed middle-cortex formation, usually at the two protoxylem poles (Fig. 6E).

We also expected that the intensity of auxin flow into the meristem would be higher in *yuc-1D* plants that have enhanced auxin synthesis rates (Zhao et al., 2001). Indeed, in half of tested 5 dag *yuc-1D* plants ($n = 10$) we detected precocious divisions of the QC and disturbed cortex/endodermis initials, although no middle-cortex cells were observed at this developmental stage (Fig. 6I). Importantly, a similar phenotype (enlarged distal meristem and no middle cortex) was detected in half of SA-accumulating mutants *dnd1* and *dnd2* at 5 dag ($n = 10$; Fig. 6, J and K), indicating that not only exogenous but also endogenous SA possesses morphogenetic effects in the root meristem.

Together our data suggest that low-level SA fine-tunes auxin distribution in the root meristem, accumulating auxin in the outer layers and the distal meristem, and by this way induces meristem maturation.

SA Affects Root Apical Meristem Radial Patterning in a *CYCD6;1*-Dependent Manner

The known mechanism of middle-cortex formation in the root includes three factors: SCARECROW (SCR), SHORT-ROOT (SHR), and CYCD6;1 (Paquette and Benfey, 2005; Sozzani et al., 2010; Koizumi et al., 2012b). We studied expression of these factors in *CYCD6;1::GFP*, *SCR::GFP*, and *SHR::SHR-GFP* plants transferred at 3 dag to liquid medium containing 30 μM SA. To detect successive formation of middle cortex the duration of treatment was set to 36 h. Despite no changes in *SCR* expression in endodermal cells after SA treatment, SHR and *CYCD6;1* expression patterns were significantly affected by SA (Fig. 7). Control plants showed a high nuclear SHR-GFP signal in endodermis cells (Fig. 7A), likely resulting in suppression of CYCD6;1 activity and reduction of periclinal cell divisions in this cell layer (Sozzani et al., 2010; Koizumi et al., 2012a, 2012b). Nuclear SHR-GFP level in the endodermis of SA-treated roots was much lower in comparison with the control (Fig. 7A). High SHR level inhibits CYCD6;1, whereas an intermediate SHR level activates CYCD6;1 (Koizumi et al., 2012a,2012b). In response to lowered SHR level, the tissue area exhibiting *CYCD6;1* expression was significantly enlarged and the *CYCD6;1* expression level increased (Fig. 7C; Supplemental Fig. S7E). These data are consistent with an SCR-SHR–dependent induction of middle cortex cell formation by SA, which activates *CYCD6;1* expression in endodermis cells. Weak *CYCD6;1* expression was detected in cortex and epidermis, suggesting that the cyclin mediates tangential cell divisions in the outer layers as well.

DISCUSSION

SA is a well-known stress hormone in plants, accumulating after pathogen attack. Basal SA concentration

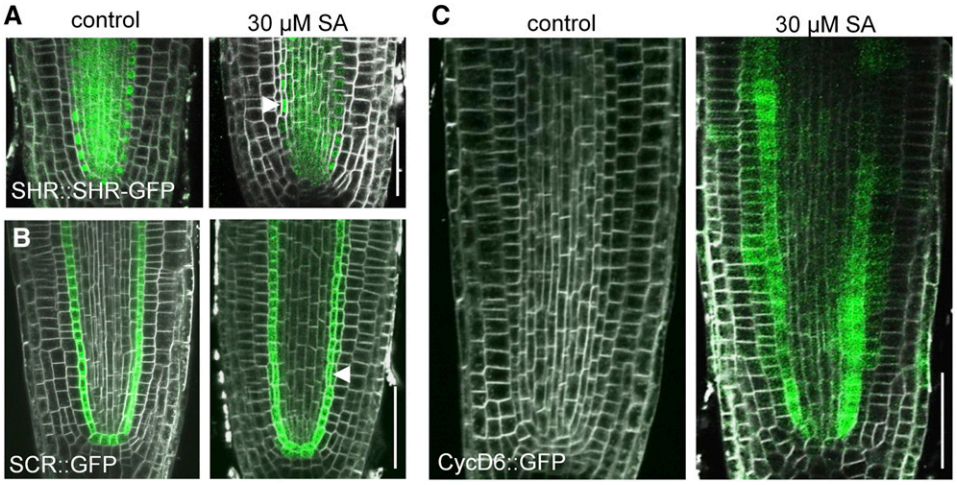

Figure 7. SA (30 μM) influences precocious formation of the middle cortex in the root meristem via a SCR-SHR-CYCD6-dependent mechanism. Three dag seedlings were transferred to liquid media containing 30 μM SA or mock. The results of a 36-h exposure to SA are shown in comparison with control roots. A, Decrease of endodermal SHR-GFP signal in SA-treated versus control roots. B, *SCR::GFP* expression in control (left) and SA-treated (right) roots. C, SA leads to enlargement of the *CYCD6;1::GFP* expression domain. A–C, Counterstained with FM4-64 Dye. White arrows indicate middle cortex formation events. Scale bars = 50 μm.

is low, ranging from 250 ng to 1 μg g^{-1} (Fresh Weight) in Arabidopsis (Rivas-San Vicente and Plasencia, 2011). Studies on Arabidopsis have been mainly associated with plant innate immunity, biasing investigations into the molecular mechanisms of SA defense action. Accordingly, only the effects of relatively high concentrations of exogenous SA (>50 μM) have been studied in depth on Arabidopsis, and mainly on aerial portions of plants (Cao et al., 1997; Fu et al., 2012; Matoušková et al., 2014; Xu and Brosché, 2014). The influence of SA on root systems has been studied to a lesser extent. SA-induced inhibition of root growth with enhanced root waving was shown in Arabidopsis for relatively low concentrations (Zhao et al., 2015). The inhibitory effect was also demonstrated for high SA dosages (Iglesias et al., 2011; Armengot et al., 2014; Sašek et al., 2014).

SA Effect on Root Growth Is Concentration Dependent

Statistical analysis of root growth changes in seedlings exposed to exogenous SA (Fig. 1) allows us to distinguish concentration ranges, which induce different responses in the meristem (Fig. 8). We identify two roles of SA: first as a developmental regulator and second as a stress hormone. At concentrations below 50 μM, SA induces distal meristem enlargement, inhibition of lateral root development, and activation of adventitious roots (Figs. 1 and 2; Supplemental Fig. S1). These physiological effects are mediated by auxin redistribution and a greater auxin response in the root tip (Fig. 4), but do not require PR1-signaling in the RAM (Fig. 3B).

Above 100 μM, exogenous SA treatment induces PR1 and SAR in the elongation and maturation zone, a process mediated by the NPR1-signaling pathway (Fu and Dong, 2013). At these dosages, SA inhibits cell proliferation and elongation in the root (Figs. 1, 2, and 3A) in a zone spatially distinct from PR1 induction (Fig. 3B). Because the root meristem structure is maintained during exposure to 150 μM SA, but its cell sizes greatly increase (Fig. 2C), we can conclude that high-dosage SA inhibits cell cycle progression making the meristem quiescent. After 5 d of SA treatment, the meristem was still able to restore root growth if transferred to mock medium. Inhibition of meristem activity happens in parallel with auxin depletion in the root tip (Fig. 4, B and E).

SA Modulates Root System Architecture

Exogenous SA inhibits primary root growth at concentrations as low as 3 μM (Fig. 1A). Additionally, SA treatment decreases cell length (Fig. 1B), with dosages above 50 μM inhibiting all growth processes. In the 10–50 μM concentration window, SA inhibits lateral root initiation, while activating adventitious root development (Fig. 1, C, D, and F; Supplemental Fig. S1). In addition, low SA levels impede development of already initiated lateral root primordia in the mature zone. Importantly, this effect is from stage IV and older primordia (Supplemental Fig. S1), wherein the typical root meristem auxin pattern starts to be formed (Benková et al., 2003). We hypothesize that SA-induced auxin accumulation inhibits progression of lateral root development.

SA treatment, therefore, results in the development of a shallow root system with a short primary root, fewer lateral roots, and well-developed adventitious

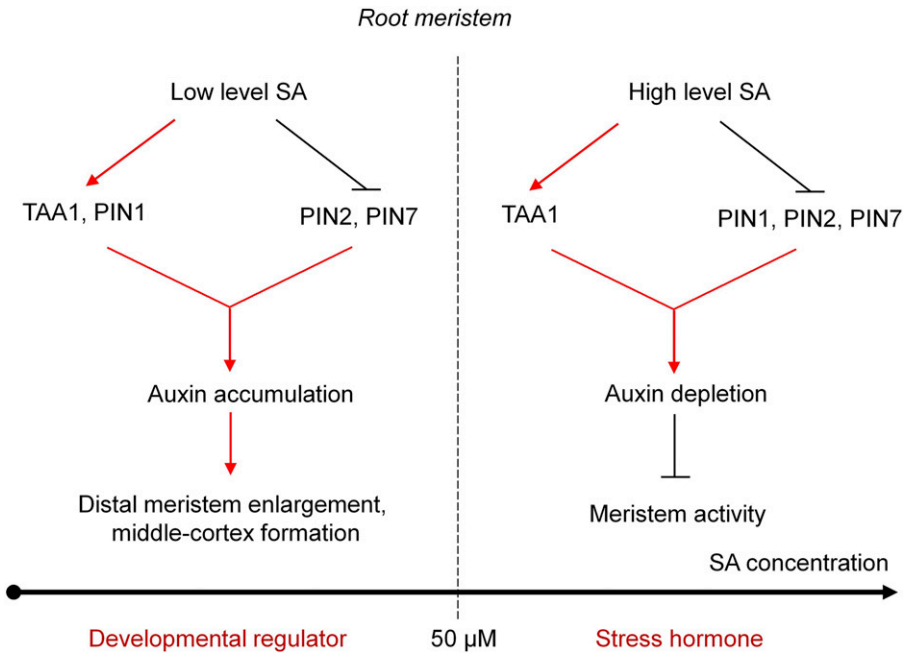

Figure 8. Concentration-dependent mechanisms of SA action on the root meristem. Low-level (below 50 μM), exogenous SA acts as a developmental regulator in Arabidopsis root meristems, but at high levels (above 50 μM) SA acts as a stress hormone. Low-level SA activates (red arrow) PIN1 and TAA1, but represses (black T-bar) PIN2 and PIN7. The net effect is middle cortex induction and distal meristem enlargement through auxin accumulation. High-level SA activates TAA1 and represses PIN1, PIN2, and PIN7, which together deplete auxin from the stem cell niche. Cell division activity of the meristem is inhibited, a reversible effect upon transfer to SA-free medium.

and secondary adventitious roots. This developmental scenario might be the norm in other plant species, which have higher endogenous SA. Although this hypothesis remains to be tested, we know that SA activates adventitious root growth in pea (*Pisum sativum*) as well (Yang et al., 2013) and that an SA-deficient mutant in rice has reduced root meristem activity (Xu et al., 2017). An SA-induced increase in root biomass was shown for *Pinus patula* (San-Miguel et al., 2003), soybean (Gutiérrez-Coronado et al., 1998), and corn (Agtuca et al., 2013). An interesting study on induction of root growth by femtomolar concentrations of exogenous SA in roots of *C. roseus* transformed by *Agrobacterium rhizogenes* (Echevarría-Machado et al., 2007) showed that root biomass increased due to enhanced lateral root growth and reduced distance between the root tip and the nearest lateral root primordia.

SA inhibits root elongation at all concentrations tested (Fig. 1A). The shorter cells in roots exposed to SA (Fig. 1B) presumably are due to their quicker passage through the elongation zone. Analysis of TAA1 activity suggests auxin accumulation in the epidermis of the distal elongation zone in roots exposed to SA (Fig. 4D), which can explain this effect. Induction of TAA1 in this zone in response to Al stress greatly enhances local DR5 expression and inhibits root elongation (Yang et al., 2014).

In contrast with lateral roots, the initiation of adventitious roots is stimulated by high cellular auxin concentration (Ludwig-Müller et al., 2005). DR5 signal is consistently observed throughout the length of the root treated by 30 μM SA, including the root-to-shoot junction (Supplemental Fig. S2, A and B). Two main regulators of adventitious rooting in Arabidopsis have been proposed: auxin and jasmonic acid (JA). Whereas auxin activates adventitious rooting in a wide range of concentrations, JA inhibits it (Gutierrez et al., 2012). It has previously been shown that the levels of GH3.3, GH3.5, and GH3.6, which conjugate SA, JA, and indole-3-acetic acid (IAA) in vitro, were correlated with the number of adventitious roots (Staswick et al., 2005; Sorin et al., 2006; Gutierrez et al., 2012). The present results reinforce SA as an important player of the regulatory mechanism for adventitious rooting. As the basal content of SA significantly varies between different plant species (Raskin et al., 1990), study of SA-IAA-JA crosstalk may shed light on the mechanisms of transition between development of taproot and fibrous root systems.

SA Induces RAM Maturation, Affecting Both Longitudinal and Radial RAM Structure

A high-resolution study of the root apical meristem in SA-treated plants shows changes in longitudinal and radial patterning (Figs. 2 and 6; Supplemental Fig. S7, B–D). One of the most remarkable effects of SA is the enlargement of the distal meristem (Fig. 2D), which is the phenotype previously reported for the lines overexpressing the genes responsible for root cap specification, such as *35S:WOX5-GR* (Sarkar et al., 2007), *35S::mir160* (Wang et al., 2005), and *35S::SHR-GFP* (Yu et al., 2017). Here we also described a slight disturbance in division of cortex/endodermis initials and precocious QC divisions in the dominant mutant *yuc-1D* with an enhanced auxin biosynthesis (Fig. 6I) and in SA-accumulating mutants *dnd1* and *dnd2* (Fig. 6, J and K).

A slight enlargement of the distal meristem naturally occurs in older seedlings (8 dag and older; Fig. 6H). Between 7 and 14 dag Arabidopsis roots also develop the middle cortex (Baum et al., 2002; Koizumi et al.,

2012b; Fig. 6E); thus middle cortex formation is a normal process during RAM maturation. However, SA treatment induces precocious activation of the middle cortex (Fig. 6D). Exogenous SA induces multiple sites of periclinal divisions in endodermis cells of 5–7 dag roots (Fig. 6D; Supplemental Fig. S7, B–D).

Middle cortex formation depends on the SHR-SCR pathway (Koizumi et al., 2012a). Treatment with 30 μM SA leads to a decrease in the amount of nuclear SHR in endodermis cells (Fig. 7A), which results in an enlarged domain of *CYCD6;1* expression (Fig. 7C; Supplemental Fig. S7E). It is important to note that these changes occur in the background of increased auxin content in the RAM (Fig. 4A; Supplemental Fig. S2), which indirectly supports the previously established link between auxin and *CYCD6;1* expression (Cruz-Ramírez et al., 2012). Distal meristem enlargement and middle cortex formation in response to SA in our experiments suggest that in Arabidopsis low-level SA promotes RAM maturation. We can speculate that in species with enlarged QCs and thick ground tissues , low-level SA signaling may mediate normal root development.

SA Modifies Auxin Distribution in the Root Tip

Previous literature supports an effect of SA on auxin content in the root. Auxin accumulation upon 50 μM SA treatment was described in wheat roots (Shakirova et al., 2003) and surmised in Arabidopsis roots (Pasternak et al., 2005). A DR5 signal depletion was detected in Arabidopsis roots upon 100–200 μM SA (Wang et al., 2007), but Zhao et al. (2015) also reported a decrease in DR5 expression in the root tip upon 30 μM SA treatment. Even though 50–200 μM SA treatment inhibits GFP fluorescence (de Jonge et al., 2017), we consistently observe an increase in DR5::GFP fluorescence after 30 μM SA treatment. The results of de Jonge et al. (2017) showed that the GFP in protein fusions, but not purified GFP, is affected by SA. However, the fact that DR5::GFP codes for free GFP does not explain this inconsistency, as we observe that TAA1:TAA1-GFP, a protein fusion, also shows an increase after SA treatment. A likely explanation is that our reporters express high amounts of GFP, and are less affected by SA than reporters with low amounts of GFP. Because we consistently see increases or decreases in DR5 reporters depending on the reporter and treatment combination (Fig. 4, A and B; Supplemental Fig. S2, A–D), we are confident of our reporter quantifications. We carefully document the effects of different SA concentrations on DR5 expression and provide semiquantitative analysis showing that low-level SA significantly enhances DR5 expression, whereas high-level SA leads to depletion of DR5 signal (Fig. 4, A, B, and E). We show that low-level SA upregulates TAA1 and PIN1 expression and downregulates PIN2 and PIN7 expression. In contrast, high levels of SA up-regulate TAA1 and down-regulate the auxin transporters (Fig. 4, C and D, and 8).

To date only negative effects of SA (or its analog Benzothiadiazole [BTH]) on auxin transport and response has been reported (Du et al., 2013; Armengot et al., 2014; Zhao et al., 2015). The inhibitory action of 30 μM SA on PIN2, PIN3, and PIN7 in the root tip (Zhao et al., 2015) is in agreement with our data. However, Armengot et al. (2014) use a high (250 μM) SA concentration, and measure only transcriptional output, making a direct comparison to our results impossible. The effect of low-level SA might be mediated at the posttranscriptional level, as 15–50 μM SA interferes with PIN1 and PIN2 clathrin-mediated internalization, which does not depend on transcription or protein synthesis (Du et al., 2013; Rong et al., 2016). The SA effect on clathrin-mediated endocytosis is independent of the known NPR3/NPR4 pathway (Rong et al., 2016).

Global repression of auxin-related genes by 60 μM BTH, including the *TIR1* (*TRANSPORT INHIBITOR RESPONSE 1*) auxin receptor, was detected by Wang et al. (2007). Exogenous SA (1 mM) has the same effect on *TIR1* expression (Iglesias et al., 2011). It was concluded that by limiting auxin receptors, SA stabilized Aux/IAA proteins and interfered with auxin response. However, the inhibitory effect of 60 μM BTH was shown to be a part of the SA-mediated disease-resistance mechanism, which was not the case for the low-level SA treatments in our study.

When we compare our data with those previously published, it is clear that there is a gap in understanding the cross talk between auxin and SA. Rigorous studies of transcriptional and posttranscriptional effects of low-level SA would be needed.

The Developmental Aspects of SA Action on the Root Involve Auxin Transport and Synthesis

The next question to address is whether SA-induced changes in auxin transport and synthesis (Fig. 4E) are responsible for selective auxin accumulation or depletion at the sites of SA action, where tissue patterning occurs (Fig. 2). Mathematical modeling has become an eligible approach to study mechanistic behavior of auxin and its role in root growth and development (for review, see Goh et al., 2014). A number of existing models with prepositioned PIN proteins are capable to predict auxin patterning in the root tip (e.g. Moore et al., 2015; van den Berg et al., 2016; Xuan et al., 2016). However, given that SA affects PIN expression, we had to consider that auxin feeds back on PIN expression patterns as well, requiring that we build on our earlier model (Mironova et al., 2012; Hong et al., 2017). The current model reshapes PIN expression domains in response to external and internal stimuli, giving an unprecedented potential to study the dynamic influence of factors on root meristem patterning. By simulating the SA influence on auxin synthesis and transport, we show that its effect on auxin distribution is balanced, supporting maintenance of the distal auxin maximum; low-level SA increases auxin amount around the distal maximum, whereas high-level SA decreases it (Fig. 5, D–F).

We suggest that adjustment of auxin distribution in the root tip shown in vivo and explored in silico for both low and high levels of SA causes the observed phenotypic changes in the root (Fig. 8). Because a larger portion of the root tip under low-level SA treatment has cellular auxin concentrations that sufficient to maintain the QC and columella initials (Figs. 4A and 5, D and E), the distal meristem becomes enlarged. An increase in cellular auxin concentration in the outer cell layers (Supplemental Fig. S7A) is able to explain extra periclinal cell divisions there (Fig. 6B). The model predicts that auxin concentration in the endodermal cell layer would be higher after low-level SA exposure when compared with those in epidermis and cortex cells (Supplemental Fig. S7A); this may explain why extra periclinal divisions occurred in endodermis cells more often. On the other hand, predicted auxin amounts for vascular cells in the roots treated by both low and high levels of SA were lower when compared with the control, which may explain why there were less vascular cell files in the roots grown under SA treatment.

The mathematical model not only detailed the auxin distribution pattern in the root meristem of SA-treated roots, but also predicted that enhanced auxin inflow to the meristem (observed in the older plants or in *yuc-1D* plants) mimic a low-level SA effect .

CONCLUSION

The results presented here show that SA influences root meristem structure and root system architecture in Arabidopsis in a concentration-dependent manner. The effects are mediated by changes in auxin synthesis, distribution, and response, but do not appear to involve PR1-signaling in the RAM. The literature supports these observations and conclusions in several plant species. Further studies should be undertaken to test whether endogenous variation in SA metabolism and concentration among species plays a role in the diversity of root meristem organizations and root system architectures observed in nature.

MATERIALS AND METHODS

Plant Materials

The plant varieties used in these experiments are the following; (1) Arabidopsis (*Arabidopsis thaliana* accession Col-0 Heyhn., (2) mutants *dnd1* and *dnd2* (NASC 6523, 6524; Clough et al., 2000; Jurkowski et al., 2004), *yuc-1D* (Zhao et al., 2001); (3) reporter lines *PR1::GUS* (Shapiro and Zhang, 2001); *DR5::GUS* and *DR5::GFP* (Ulmasov et al., 1997; Ottenschläger et al., 2003), *CYCB1;1::GUS* (Colón-Carmona et al., 1999), *CYCD6;1::GFP* (Sozzani et al., 2010), *pDR5rev::3XVENUS-N7 + pPIN1::PIN1-GFP* (Heisler et al., 2005), *PIN1::PIN1-GFP, PIN2::PIN2-GFP, PIN7::PIN7-GFP* (Vieten et al., 2005), *SHR::SHR-GFP* (Nakajima et al., 2001), *SCR::GFP* (Sabatini et al., 1999), *TAA1::TAA1-GFP* (Stepanova et al., 2008), *WOX5::GFP* (Ditengou et al., 2008).

Growth Conditions and Treatments

Seeds were surface-sterilized and sown on solid Arabidopsis medium (AM; one-half strength Murashige and Skoog containing 1% Suc [w/v], 5 mM MES, and 1.1% agar [w/v], pH 5.6 adjusted with KOH). After vernalization for 16 h at 4°C, seeds were germinated on vertically oriented plates under 16:8 h light:dark period with a light intensity of 80 μmol $s^{-1}m^{-2}$. The 4-d-old plants grown on AM medium were transferred to solid AM supplemented with SA (S7401, Sigma-Aldrich) at different concentrations (0, 3, 10, 20, 30, 50, 100, 150, and 200 μM), 5 μM *l*-kynurenine, or 5 μM NPA. After transfer, plants were grown for 2–5 d in studies of root length, root tip anatomy, and fluorescence quantification. Short-term SA treatments (< 36 h) were performed in liquid AM supplemented with 30 or 150 μM SA.

Whole-Mount in Situ Immunolocalization

Immunolocalization in Arabidopsis plants was performed according to a whole-mount in situ protocol (Pasternak et al., 2015). Affinity-purified primary anti-PIN1 (mouse, clone 7E7F), anti-PIN2 (guinea pig, clone 192), and anti-PIN4 (rabbit, clone 9105) antibodies were diluted 1:40, 1:400, and 1:400 and 1:400, respectively. The secondary Alexa-488/Alexa 555 conjugated antiguinea pig, antirabbit, or antimouse antibodies were diluted 1:400.

Microscopy

Histological detection of β-glucuronidase (GUS) activity was performed according to a standard protocol. Plants were mounted in 50% (v/v) glycerol and observed with a Zeiss Axiovert 200M MOT (Carl Zeiss MicroImaging).

Analysis of the fluorescent signal in vivo was done with a Zeiss Stemi SV11 APO stereomicroscope equipped with an HBO lamp and a GFP filter set (488 nm excitation and 530–550 nm emission). For high-resolution images, plants containing fluorescent markers were fixed with 4% formaldehyde (v/v) and mounted in Prolong Gold antifade reagent containing 4′,6-diamino-phenylindole (DAPI; Molecular Probes). Fluorescent proteins were analyzed with a Zeiss LSM 5 *DUO* scanning microscope in living root. Seedlings were incubated in the liquid medium containing 1 μM N-(3-Triethylammoniumpropyl)-4-(6-(4-(Diethylamino) Phenyl) Hexatrienyl) Pyridinium Dibromide (FM4-64) for 20 minutes. To monitor GFP and FM4-64 fluorescence, we used multitracking in frame mode. GFP was excited using the 488 nm laser line in conjunction with a 505–530 band-pass filter. FM4-64 was excited with the 561 nm laser line and collected using a 575 nm band-pass filter.

The RAM anatomy was analyzed according to Truernit et al., 2008 with some modifications. Plants were fixed with 4% (v/v) formaldehyde in MTSB (microtubule stabilization buffer), treated with methanol, periodic acid (P7875, Sigma-Aldrich) and propidium iodide (P4170, Sigma-Aldrich) in the presence of sodium bisulfite at pH 1.4.

Image Analysis

For root growth analysis the petri dishes were scanned with a Canon 950 scanner. Quantitative analysis of root length, width, and fluorescence intensity was done using ImageJ (Schneider et al., 2012). The fluorescent intensity was measured as mean and maximal gray levels in the green channel per area. The area was defined as the root tip up to QC for *DR5*, PIN7, and TAA1 expression level measurements and the RAM portion from the QC up to 150 μm above for PIN1 and PIN2 levels. Images from the confocal microscope were analyzed with the ZEN image browser (Carl Zeiss MicroImaging).

Mathematical Modeling

A study of the SA effect on auxin distribution in the root meristem was done using an adapted model (Mironova et al., 2012) in MatLab software. The model describes auxin ($Auxin_{ij}$) distribution through a 2D cell layout (i=1…25 and j=1…10). Five cell layers are considered in the model: epidermis (j=1,10); cortex (j=2,9), endodermis (j=3,8), pericycle (j=4,7) and vascular cells (j=5–6). The cell layers differ by PINs expression (Fig. 4A). The cells located at the root tip have i=1; those located at the border of the meristem have i = 25. There are two auxin sources in the meristem: (1) auxin inflow to vascular and pericycle cells (i=25; j=4…7); and (2) de novo auxin synthesis in all the cells of the layout. Auxin distributes in the cellular layout by diffusion and PIN-mediated active transport. Depending on concentration, auxin regulates PIN synthesis and degradation: PIN2 is upregulated by the lowest auxin concentrations, PIN1 by intermediate and PIN7 by the highest (see Mironova et al., 2012) for details). For simplicity, all synthesized PIN proteins are located on the membrane with the predefined polarities according to the experimental data (Fig. 4A). SA action on

auxin distribution was simulated by altering the rates for auxin and PINs synthesis, according to the experimental data (Figs. 4E and 5, B and C; see Hong et al. [2017] and Supplemental Text for details). For comparison with experimentally observed results, average concentrations were determined in the steady state solution as follows: $i=1\ldots4$ for DR5, PIN7, and TAA1 and $i=10\ldots20$ for PIN1 and PIN2.

Statistical Analysis

Statistical differences were assessed by one-way ANOVA with Tukey post hoc test using *agricolae* R package. Different letters in graphs denote statistical differences at p-value < 0.05.

Accession Numbers

Accession numbers of the genes mentioned in this study are: *CYCB1;1* (AT4G37490), *CYCD6;1* (AT4G03270), *DND1* (AT5G15410), *DND2* (AT5G54250), *GH3.3* (AT2G23170), *GH3.5* (AT4G27260), *GH3.6* (AT5G54510), *mir-160a* (AT2G39175), *mir-160b* (AT4G17788), *mir-160c* (AT5G46845), *NPR1* (AT1G64280), *NPR3* (AT5G45110), *NPR4* (AT4G19660), *PIN1* (AT1G73590), *PIN2* (AT5G57090), *PIN3* (AT1G70940), *PIN4* (AT2G01420), *PIN7* (AT1G23080), *PR1* (AT2G14610), *SCR* (AT3G54220), *SHR* (AT4G37650), *TAA1* (AT1G70560), *TIR1* (AT3G62980), *WOX5* (AT3G11260), and *YUC1* (AT4G32540).

Supplemental Data

The following supplemental materials are available.

Supplemental Figure S1. Lateral root primordium development after transfer of 3 dag seedlings to media containing 0, 3, 10, or 30 μM SA for 5 d.

Supplemental Figure S2. SA effects on the reporters activity in *DR5::VENUS, DR5::GUS* and *TAA1::TAA1-GFP* 5 dag plants.

Supplemental Figure S3. Steady-state solutions of the mathematical model for control and 30 μM SA treatment.

Supplemental Figure S4. Mathematical modeling of 150 μM SA action on auxin distribution in the root tip.

Supplemental Figure S5. Exploration of individual parameters in the mathematical model.

Supplemental Figure S6. Exploration of the auxin synthesis rate parameter versus the auxin inflow and PINs expression parameters in the mathematical model.

Supplemental Figure S7. 3-Dimensional analysis of root tip structure after exposure to 30 μM SA.

Supplemental Table S1. Parameter settings used in the model to simulate auxin distribution in the root tip of control and SA-treated roots.

Supplemental Text. Mathematical model description.

ACKNOWLEDGMENTS

This work could not have been accomplished without the help of Thorsten Schmidt, Thomas Haser, and Franck Ditengou who provided support, suggestions, and materials. We also gratefully acknowledge excellent technical support from Roland Nitschke, Elena Ubogoeva, and Daria Novikova, Viktoriya Lavrekha. The numerical simulations were performed on the Core center facility "Bioinformatics" of the Siberian Supercomputer Center RAS. V.V.M. gratefully acknowledges Dmitri Zimin and his Dynasty Foundation for support in the beginning of the project without which the work would not have been done.

Received January 31, 2019; accepted April 17, 2019; published April 29, 2019.

LITERATURE CITED

Agtuca B, Rieger E, Hilger K, et al (2013) Carbon-11 reveals opposing roles of auxin and salicylic acid in regulating leaf physiology, leaf metabolism, and resource allocation patterns that impact root growth in *Zea mays*. J Plant Growth Regul **33:** 328–339

Armengot L, Marquès-Bueno MM, Soria-Garcia A, Müller M, Munné-Bosch S, Martínez MC (2014) Functional interplay between protein kinase CK2 and salicylic acid sustains PIN transcriptional expression and root development. Plant J **78:** 411–423

Baum SF, Dubrovsky JG, Rost TL (2002) Apical organization and maturation of the cortex and vascular cylinder in *Arabidopsis thaliana* (Brassicaceae) roots. Am J Bot **89:** 908–920

Benková E, Michniewicz M, Sauer M, Teichmann T, Seifertová D, Jürgens G, Friml J (2003) Local, efflux-dependent auxin gradients as a common module for plant organ formation. Cell **115:** 591–602

Bhalerao RP, Eklöf J, Ljung K, Marchant A, Bennett M, Sandberg G (2002) Shoot-derived auxin is essential for early lateral root emergence in *Arabidopsis* seedlings. Plant J **29:** 325–332

Cao H, Glazebrook J, Clarke JD, Volko S, Dong X (1997) The Arabidopsis NPR1 gene that controls systemic acquired resistance encodes a novel protein containing ankyrin repeats. Cell **88:** 57–63

Clough SJ, Fengler KA, Yu IC, Lippok B, Smith RK, Jr., Bent AF (2000) The Arabidopsis dnd1 "defense, no death" gene encodes a mutated cyclic nucleotide-gated ion channel. Proc Natl Acad Sci USA **97:** 9323–9328

Colón-Carmona A, You R, Haimovitch-Gal T, Doerner P (1999) Technical advance: Spatio-temporal analysis of mitotic activity with a labile cyclin-GUS fusion protein. Plant J **20:** 503–508

Cruz-Ramírez A, Díaz-Triviño S, Blilou I, Grieneisen VA, Sozzani R, Zamioudis C, Miskolczi P, Nieuwland J, Benjamins R, Dhonukshe P, Caballero-Pérez J, Horvath B, et al (2012) A bistable circuit involving SCARECROW-RETINOBLASTOMA integrates cues to inform asymmetric stem cell division. Cell **150:** 1002–1015

de Jonge J, Hofius D, Hennig L (2017) Salicylic acid interferes with GFP fluorescence in vivo. J Exp Bot **68:** 1689–1696

Della Rovere F, Fattorini L, D'Angeli S, Veloccia A, Falasca G, Altamura MM (2013) Auxin and cytokinin control formation of the quiescent centre in the adventitious root apex of Arabidopsis. Ann Bot **112:** 1395–1407

Ding Z, Friml J (2010) Auxin regulates distal stem cell differentiation in Arabidopsis roots. Proc Natl Acad Sci USA **107:** 12046–12051

Ditengou FA, Teale WD, Kochersperger P, Flittner KA, Kneuper I, van der Graaff E, Nziengui H, Pinosa F, Li X, Nitschke R, et al (2008) Mechanical induction of lateral root initiation in Arabidopsis thaliana. Proc Natl Acad Sci USA **105:** 18818–18823

Du Y, Tejos R, Beck M, Himschoot E, Li H, Robatzek S, Vanneste S, Friml J (2013) Salicylic acid interferes with clathrin-mediated endocytic protein trafficking. Proc Natl Acad Sci USA **110:** 7946–7951

Echevarría-Machado I, Escobedo-G M RM, Larqué-Saavedra A (2007) Responses of transformed Catharanthus roseus roots to femtomolar concentrations of salicylic acid. Plant Physiol Biochem **45:** 501–507

Fariduddin Q, Hayat S, Ahmad A (2003) Salicylic acid influences net photosynthetic rate, carboxylation efficiency, nitrate reductase activity, and seed yield in *Brassica juncea*. Photosynthetica **41:** 281–284

Fu ZQ, Dong X (2013) Systemic acquired resistance: Turning local infection into global defense. Annu Rev Plant Biol **64:** 839–863

Fu ZQ, Yan S, Saleh A, Wang W, Ruble J, Oka N, Mohan R, Spoel SH, Tada Y, Zheng N, et al (2012) NPR3 and NPR4 are receptors for the immune signal salicylic acid in plants. Nature **486:** 228–232

Goh T, Voβ U, Farcot E, Bennett MJ, Bishopp A (2014) Systems biology approaches to understand the role of auxin in root growth and development. Physiol Plant **151:** 73–82

Gutierrez L, Mongelard G, Floková K, Pacurar DI, Novák O, Staswick P, Kowalczyk M, Pacurar M, Demailly H, Geiss G, et al (2012) Auxin controls Arabidopsis adventitious root initiation by regulating jasmonic acid homeostasis. Plant Cell **24:** 2515–2527

Gutiérrez-Coronado MA, Trejo-López C, Larqué-Saavedra A (1998) Effects of salicylic acid on the growth of roots and shoots in soybean. Plant Physiol Biochem **36:** 563–565

Hayat S, Fariduddin Q, Ali B, Ahmad A (2005) Effect of salicylic acid on growth and enzyme activities of wheat seedlings. Acta Agron Hung **53:** 433–437

Heisler MG, Ohno C, Das P, Sieber P, Reddy GV, Long JA, Meyerowitz EM (2005) Patterns of auxin transport and gene expression during primordium development revealed by live imaging of the Arabidopsis inflorescence meristem. Curr Biol **15:** 1899–1911

Hong JH, Savina M, Du J, Devendran A, Kannivadi Ramakanth K, Tian X, Sim WS, Mironova VV, Xu J (2017) A sacrifice-for-survival mechanism protects root stem cell niche from chilling stress. Cell **170:** 102–113.e14

Hosseini SS, Mashayekhi K, Alizadeh M, Ebrahimi P (2011) Effect of salicylic acid on somatic embryogenesis and chlorogenic acid levels of carrot (*Daucus carota cv. Nantes*) explants. J Ornam Hortic Plants **1:** 105–113

Iglesias MJ, Terrile MC, Casalongué CA (2011) Auxin and salicylic acid signalings counteract the regulation of adaptive responses to stress. Plant Signal Behav **6:** 452–454

Jurkowski GI, Smith RK, Jr., Yu IC, Ham JH, Sharma SB, Klessig DF, Fengler KA, Bent AF (2004) *Arabidopsis DND2,* a second cyclic nucleotide-gated ion channel gene for which mutation causes the "*defense, no death*" phenotype. Mol Plant Microbe Interact **17:** 511–520

Koizumi K, Hayashi T, Gallagher KL (2012a) SCARECROW reinforces SHORT-ROOT signaling and inhibits periclinal cell divisions in the ground tissue by maintaining SHR at high levels in the endodermis. Plant Signal Behav **7:** 1573–1577

Koizumi K, Hayashi T, Wu S, Gallagher KL (2012b) The SHORT-ROOT protein acts as a mobile, dose-dependent signal in patterning the ground tissue. Proc Natl Acad Sci USA **109:** 13010–13015

Kovácik J, Grúz J, Backor M, Strnad M, Repcák M (2009) Salicylic acid-induced changes to growth and phenolic metabolism in *Matricaria chamomilla* plants. Plant Cell Rep **28:** 135–143

Ludwig-Müller J, Vertocnik A, Town CD (2005) Analysis of indole-3-butyric acid-induced adventitious root formation on Arabidopsis stem segments. J Exp Bot **56:** 2095–2105

Matoušková J, Janda M, Fišer R, Sašek V, Kocourková D, Burketová L, Dušková J, Martinec J, Valentová O (2014) Changes in actin dynamics are involved in salicylic acid signaling pathway. Plant Sci **223:** 36–44

Mironova VV, Omelyanchuk NA, Novoselova ES, Doroshkov AV, Kazantsev FV, Kochetov AV, Kolchanov NA, Mjolsness E, Likhoshvai VA (2012) Combined in silico/in vivo analysis of mechanisms providing for root apical meristem self-organization and maintenance. Ann Bot **110:** 349–360

Miura K, Tada Y (2014) Regulation of water, salinity, and cold stress responses by salicylic acid. Front Plant Sci **5:** 4

Moore S, Zhang X, Mudge A, Rowe JH, Topping JF, Liu J, Lindsey K (2015) Spatiotemporal modelling of hormonal crosstalk explains the level and patterning of hormones and gene expression in *Arabidopsis thaliana* wild-type and mutant roots. New Phytol **207:** 1110–1122

Mur LAJ, Kenton P, Atzorn R, Miersch O, Wasternack C (2006) The outcomes of concentration-specific interactions between salicylate and jasmonate signaling include synergy, antagonism, and oxidative stress leading to cell death. Plant Physiol **140:** 249–262

Nakajima K, Sena G, Nawy T, Benfey PN (2001) Intercellular movement of the putative transcription factor SHR in root patterning. Nature **413:** 307–311

Ottenschläger I, Wolff P, Wolverton C, Bhalerao RP, Sandberg G, Ishikawa H, Evans M, Palme K (2003) Gravity-regulated differential auxin transport from columella to lateral root cap cells. Proc Natl Acad Sci USA **100:** 2987–2991

Paquette AJ, Benfey PN (2005) Maturation of the ground tissue of the root is regulated by gibberellin and SCARECROW and requires SHORT-ROOT. Plant Physiol **138:** 636–640

Pasternak T, Rudas V, Potters G, Jansen MAK (2005) Morphogenic effects of abiotic stress: Reorientation of growth in Arabidopsis thaliana seedlings. Environ Exp Bot **53:** 299–314

Pasternak T, Tietz O, Rapp K, Begheldo M, Nitschke R, Ruperti B, Palme K (2015) Protocol: An improved and universal procedure for whole-mount immunolocalization in plants. Plant Methods **11:** 50

Raskin I, Skubatz H, Tang W, Meeuse BJD (1990) Salicylic acid levels in thermogenic and non-thermogenic plants. Ann Bot **66:** 369–373

Rivas-San Vicente M, Plasencia J (2011) Salicylic acid beyond defence: Its role in plant growth and development. J Exp Bot **62:** 3321–3338

Rong D, Luo N, Mollet JC, Liu X, Yang Z (2016) Salicylic acid regulates pollen tip growth through an NPR3/NPR4-independent pathway. Mol Plant **9:** 1478–1491

Sabatini S, Beis D, Wolkenfelt H, Murfett J, Guilfoyle T, Malamy J, Benfey P, Leyser O, Bechtold N, Weisbeek P, et al (1999) An auxin-dependent distal organizer of pattern and polarity in the Arabidopsis root. Cell **99:** 463–472

San-Miguel R, Gutiérrez M, Larqué-Saavedra A (2003) Salicylic acid increases the biomass accumulation of *Pinus patula*. South J Appl For **27:** 52–54

Sarkar AK, Luijten M, Miyashima S, Lenhard M, Hashimoto T, Nakajima K, Scheres B, Heidstra R, Laux T (2007) Conserved factors regulate signalling in Arabidopsis thaliana shoot and root stem cell organizers. Nature **446:** 811–814

Sašek V, Janda M, Delage E, Puyaubert J, Guivarc'h A, López Maseda E, Dobrev PI, Caius J, Bóka K, Valentová O, et al (2014) Constitutive salicylic acid accumulation in pi4kIIIβ1β2 Arabidopsis plants stunts rosette but not root growth. New Phytol **203:** 805–816

Schmidt T, Pasternak T, Liu K, Blein T, Aubry-Hivet D, Dovzhenko A, Duerr J, Teale W, Ditengou FA, Burkhardt H, Ronneberger O, Palme K (2014) The iRoCS Toolbox--3D analysis of the plant root apical meristem at cellular resolution. Plant J **77:** 806–814

Schneider CA, Rasband WS, Eliceiri KW (2012) NIH Image to ImageJ: 25 Years of image analysis. Nat Methods **9:** 671–675

Shakirova FM, Sakhabutdinova AR, Bezrukova MV, et al (2003) Changes in the hormonal status of wheat seedlings induced by salicylic acid and salinity. Plant Sci **164:** 317–322

Shapiro AD, Zhang C (2001) The role of NDR1 in avirulence gene-directed signaling and control of programmed cell death in Arabidopsis. Plant Physiol **127:** 1089–1101

Sorin C, Negroni L, Balliau T, Corti H, Jacquemot MP, Davanture M, Sandberg G, Zivy M, Bellini C (2006) Proteomic analysis of different mutant genotypes of Arabidopsis led to the identification of 11 proteins correlating with adventitious root development. Plant Physiol **140:** 349–364

Sozzani R, Cui H, Moreno-Risueno MA, Busch W, Van Norman JM, Vernoux T, Brady SM, Dewitte W, Murray JA, Benfey PN (2010) Spatiotemporal regulation of cell-cycle genes by SHORTROOT links patterning and growth. Nature **466:** 128–132

Staswick PE, Serban B, Rowe M, Tiryaki I (2005) Characterization of an Arabidopsis enzyme family that conjugates amino acids to indole-3-acetic acid. Plant Cell **17:** 616–627

Stepanova AN, Robertson-Hoyt J, Yun J, Benavente LM, Xie DY, Dolezal K, Schlereth A, Jürgens G, Alonso JM (2008) TAA1-mediated auxin biosynthesis is essential for hormone crosstalk and plant development. Cell **133:** 177–191

Truernit E, Bauby H, Dubreucq B, Grandjean O, Runions J, Barthélémy J, Palauqui JC (2008) High-resolution whole-mount imaging of three-dimensional tissue organization and gene expression enables the study of Phloem development and structure in Arabidopsis. Plant Cell **20:** 1494–1503

Uknes S, Mauch-Mani B, Moyer M, Potter S, Williams S, Dincher S, Chandler D, Slusarenko A, Ward E, Ryals J (1992) Acquired resistance in Arabidopsis. Plant Cell **4:** 645–656

Ulmasov T, Hagen G, Guilfoyle TJ (1997) ARF1, a transcription factor that binds to auxin response elements. Science **276:** 1865–1868

van den Berg T, Korver RA, Testerink C, Ten Tusscher KHWJ (2016) Modeling halotropism: A key role for root tip architecture and reflux loop remodeling in redistributing auxin. Development **143:** 3350–3362

Van der Does D, Leon-Reyes A, Koornneef A, Van Verk MC, Rodenburg N, Pauwels L, Goossens A, Körbes AP, Memelink J, Ritsema T, et al (2013) Salicylic acid suppresses jasmonic acid signaling downstream of SCFCOI1-JAZ by targeting GCC promoter motifs via transcription factor ORA59. Plant Cell **25:** 744–761

Vieten A, Vanneste S, Wisniewska J, Benková E, Benjamins R, Beeckman T, Luschnig C, Friml J (2005) Functional redundancy of PIN proteins is accompanied by auxin-dependent cross-regulation of PIN expression. Development **132:** 4521–4531

Vlot AC, Dempsey DA, Klessig DF (2009) Salicylic acid, a multifaceted hormone to combat disease. Annu Rev Phytopathol **47:** 177–206

Wang D, Pajerowska-Mukhtar K, Culler AH, Dong X (2007) Salicylic acid inhibits pathogen growth in plants through repression of the auxin signaling pathway. Curr Biol **17:** 1784–1790

Wang JW, Wang LJ, Mao YB, Cai WJ, Xue HW, Chen XY (2005) Control of root cap formation by MicroRNA-targeted auxin response factors in Arabidopsis. Plant Cell **17:** 2204–2216

Xu E, Brosché M (2014) Salicylic acid signaling inhibits apoplastic reactive oxygen species signaling. BMC Plant Biol **14:** 155

Xu L, Zhao H, Ruan W, Deng M, Wang F, Peng J, Luo J, Chen Z, Yi K (2017) ABNORMAL INFLORESCENCE MERISTEM1 functions in

salicylic acid biosynthesis to maintain proper reactive oxygen species levels for root meristem activity in rice. Plant Cell **29:** 560–574

Xuan W, Band LR, Kumpf RP, Van Damme D, Parizot B, De Rop G, Opdenacker D, Möller BK, Skorzinski N, Njo MF, et al (2016) Cyclic programmed cell death stimulates hormone signaling and root development in Arabidopsis. Science **351:** 384–387

Yang W, Zhu C, Ma X, Li G, Gan L, Ng D, Xia K (2013) Hydrogen peroxide is a second messenger in the salicylic acid-triggered adventitious rooting process in mung bean seedlings. PLoS One **8:** e84580

Yang Z-B, Geng X, He C, Zhang F, Wang R, Horst WJ, Ding Z (2014) TAA1-regulated local auxin biosynthesis in the root-apex transition zone mediates the aluminum-induced inhibition of root growth in Arabidopsis. Plant Cell **26:** 2889–2904

Yu Q, Li P, Liang N, Wang H, Xu M, Wu S (2017) Cell-Fate Specification in Arabidopsis Roots Requires Coordinative Action of Lineage Instruction and Positional Reprogramming. Plant Physiol **175:** 816–827

Zhang Y, Xu S, Ding P, Wang D, Cheng YT, He J, Gao M, Xu F, Li Y, Zhu Z, et al (2010) Control of salicylic acid synthesis and systemic acquired resistance by two members of a plant-specific family of transcription factors. Proc Natl Acad Sci USA **107:** 18220–18225

Zhao X, Wang J, Yuan J, Wang XL, Zhao QP, Kong PT, Zhang X (2015) NITRIC OXIDE-ASSOCIATED PROTEIN1 (AtNOA1) is essential for salicylic acid-induced root waving in *Arabidopsis thaliana*. New Phytol **207:** 211–224

Zhao Y, Christensen SK, Fankhauser C, Cashman JR, Cohen JD, Weigel D, Chory J (2001) A role for flavin monooxygenase-like enzymes in auxin biosynthesis. Science **291:** 306–309